Observation of anomalous Hanle spin precession line shapes resulting from interaction with localized states

van den Berg, J. J.; Strupinski, W.; van Wees, B. J.

Published in:
Physical Review. B: Condensed Matter and Materials Physics

DOI:
10.1103/PhysRevB.91.081403

PHYSICAL REVIEW B **91**, 081403(R) (2015)

Observation of anomalous Hanle spin precession line shapes resulting from interaction with localized states

J. J. van den Berg,[1,*] W. Strupinski,[2] and B. J. van Wees[1]

[1]*Physics of Nanodevices, Zernike Institute for Advanced Materials, University of Groningen, Nijenborgh 4, 9747 AG Groningen, The Netherlands*

[2]*Institute of Electronic Materials Technology, Wolczynska 133, 01-919 Warsaw, Poland*

(Received 27 October 2014; revised manuscript received 16 January 2015; published 12 February 2015)

It has been shown recently that in spin precession experiments, the interaction of spins with localized states can change the response to a magnetic field, leading to a modified, effective spin relaxation time and precession frequency. Here, we show that also the shape of the Hanle curve can change, so that it cannot be fitted with the solutions of the conventional Bloch equation. We present experimental data that show such an effect arising at low temperatures in epitaxial graphene on silicon carbide with localized states in the carbon buffer layer. We compare the effect between materials made with different growth methods, epitaxial growth by sublimation and by chemical vapor deposition. The presented analysis gives information about the density of localized states and their coupling to the graphene states, which is inaccessible by charge transport measurements and can be applied to any spin transport channel that is coupled to localized states.

DOI: 10.1103/PhysRevB.91.081403 PACS number(s): 75.76.+j, 74.78.Na, 75.40.Gb

The spin relaxation length λ_S is a property that can be obtained in a (nonlocal) spin valve geometry by two independent methods: first, by measuring the spin dependent signal as a function of the distance x to the spin injecting electrode, because this signal scales with the spin accumulation $\mu_S \propto e^{-x/\lambda_S}$. The spin relaxation time τ_S is then given by $\tau_S = \lambda_S^2/D$, where D is the spin diffusion coefficient. A complementary method is Hanle spin precession, where an out-of-plane field B_z is applied to precess the spins in the x-y plane of the channel with precession frequency ω_L. D and τ_S are directly obtained by numerically fitting the Hanle curve with the stationary solutions of the one-dimensional Bloch equation,

$$\vec{0} = D\nabla^2\vec{\mu}_S - \frac{\vec{\mu}_S}{\tau_S} + \vec{\omega}_L \times \vec{\mu}_S. \quad (1)$$

Here, $\vec{\omega}_L = g\mu_B\vec{B}/\hbar$, with the Landé g factor $g = 2$, μ_B the Bohr magneton, and $\hbar$ the reduced Planck's constant.

A striking effect occurs when itinerant electron spins couple to localized spin states. The spins pick up extra relaxation and precession while residing for some time in the localized states on their way from injector to detector, as depicted in Fig. 1. This causes a significant decrease in the measured spin signal amplitude and a narrowing of the Hanle curve. The effect was observed in epitaxial graphene (EG) on silicon carbide (SiC) [1], a system that receives much interest as a platform for spin transport experiments [1–3], because of its high quality, large area, insulating substrate, and, more recently, experimental findings of room temperature ferromagnetism [4,5]. The localized states most likely originate from the buffer layer, the nonconducting graphenelike layer between the channel and substrate [6]. Though first developed for observations in EG on SiC, the localized states picture is in fact applicable to any spin transport channel which couples to localized states. Recently, Roundy and Raikh [7] theoretically studied the effect of deep traps in organic semiconductors and predicted a narrowing of the Hanle curve in a similar fashion. By making assumptions on the distribution of the dwell times in the traps, an anomalous shape of the Hanle curve was also predicted, but not yet confirmed by experiment.

In this Rapid Communication we show an anomalous line shape of the Hanle curve in spin precession experiments in EG at low temperatures. Also, we present an analysis that can qualitatively explain the observed anomalous behavior by assuming a transition regime of strong to weak coupling between the channel and the localized states. The effect is measured in EG on SiC samples that we produced by two growth methods: by sublimation [8–11] and by chemical vapor deposition (CVD) [12,13]. A difference in coupling and/or density of localized states can be expected, resulting in a measurable effect on the spin relaxation time and the precession frequency in the channel. Our analysis allows for estimating the density of localized states and the spin relaxation time for both growth methods.

We investigated two different types of EG spin valve devices: EG by sublimation (type I) and on EG by CVD (type II). We show here the results of one device of each type, and similar measurements on another type II device can be found in the Supplemental Material [14].

For both types, we grew the graphene layers at 1600°C under an argon (Ar) laminar flow in a hot-wall Aixtron VP508 reactor on semi-insulating on-axis oriented 4H-SiC(0001) substrates with dimensions 5 mm × 5 mm. The dynamic flow conditions in the reactor controlled the Si sublimation rate. For epitaxial CVD growth, we formed an Ar boundary layer thick enough to prevent Si sublimation, but allowing for the diffusion of propane gas that was led into the reactor as the precursor. The reactor pressure applied in the case of sublimation was 100 mbar and in the case of CVD 30 mbar [11,13]. These two growth methods resulted in a wafer scaled EG monolayer, with a nonconducting carbon buffer layer sandwiched between the graphene and the SiC. Raman studies showed that the buffer layer of type II has less epitaxial strain, probably due to

*j.j.van.den.berg@rug.nl

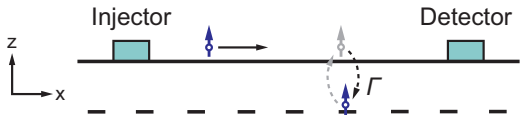

FIG. 1. (Color online) A spin transport channel coupled to localized states with a coupling rate Γ. Spins can reside in the localized states for some time, where they pick up extra relaxation and precession, thus strongly effecting the measured Hanle signal.

a different superstructure or C-C bond length. This results in slightly higher mobility than in type I, but comparable doping [13].

We produced EG spin transport devices with ferromagnetic contacts, following roughly the same recipe as described in Ref. [1]. We used electron beam lithography (EBL) to define ~ 0.5–$1.0\ \mu$m wide lines, resulting in an EG strip with a Hall cross at one end of the strip, as shown in Fig. 2(a) [15]. We used reactive ion etching in an rf O_2 plasma for 45 s (at 25 W and 0.01 mbar) for removal of the EG. In the final EBL step we defined the contact pattern. Using *e*-beam evaporation we deposited 0.9 nm of titanium oxide (TiO_2) in two steps, which we oxidized *in situ* in O_2 atmosphere after each step at a pressure above 10^{-1} mbar. The TiO_2 acts as the tunnel barrier to avoid conductivity mismatch [16,17]. Without breaking the vacuum we then deposited 40 nm of cobalt (Co) and a 5 nm aluminum (Al) capping layer to prevent the Co from oxidizing. The devices were loaded in a liquid helium flow cryostat and measured in vacuum ($\sim 10^{-7}$ mbar).

We performed room temperature Hall measurements to characterize our nanodevices, using contacts 1–4 in Fig. 2(a) [18]. We obtained a charge carrier density of $n_1 = 1.5 \times 10^{12}$ and $n_2 = 2.2 \times 10^{12}\,\mathrm{cm}^{-2}$ and a mobility of $\mu_1 = 2800$ and $\mu_2 = 2000\ \mathrm{cm}^2\ \mathrm{V}^{-1}\ \mathrm{s}^{-1}$ [19]. These values correspond to a charge diffusion coefficient $D_{C1} = 200$ and $D_{C2} = 172\mathrm{cm}^2\mathrm{s}^{-1}$ [20].

To investigate the spin transport properties we used the nonlocal spin valve geometry shown in Fig. 2(a). Using standard lock-in techniques, we sent an ac current I_{ac} (=1–5 μA) between Co contacts 6 and 7, creating a nonequilibrium spin accumulation in the channel underneath these contacts. The spin accumulation decays in both the positive and negative x direction and can be detected as a nonlocal voltage V_{nl} between spin sensitive contacts 4 and 5. A spin valve measurement consists of the nonlocal resistance $R_{\mathrm{nl}} = V_{\mathrm{nl}}/I_{\mathrm{ac}}$ as a function of an in-plane field B_y. Because of a different width of each contact and thereby a difference in their coercive fields, it is possible to switch their magnetization direction independently. A sudden change in R_{nl} can be observed when the relative orientation of the injector and detector changes from parallel to antiparallel or vice versa. When the outer contacts are far away at a distance greater than λ_S, we can neglect their influence, resulting in a typical two-level spin valve.

Figures 2(b) and 2(c) show room temperature (RT) spin valve measurements of type I ($L = 1\ \mu$m and $W = 0.85\ \mu$m) and type II ($L = 1\ \mu$m and $W = 0.62\ \mu$m). Figures 2(d) and 2(e) show RT Hanle precession experiments. Both devices show very narrow Hanle curves when compared to typical exfoliated graphene, as was already reported for type I devices in Ref. [1]. If we now use Eq. (1) to fit the experimental data

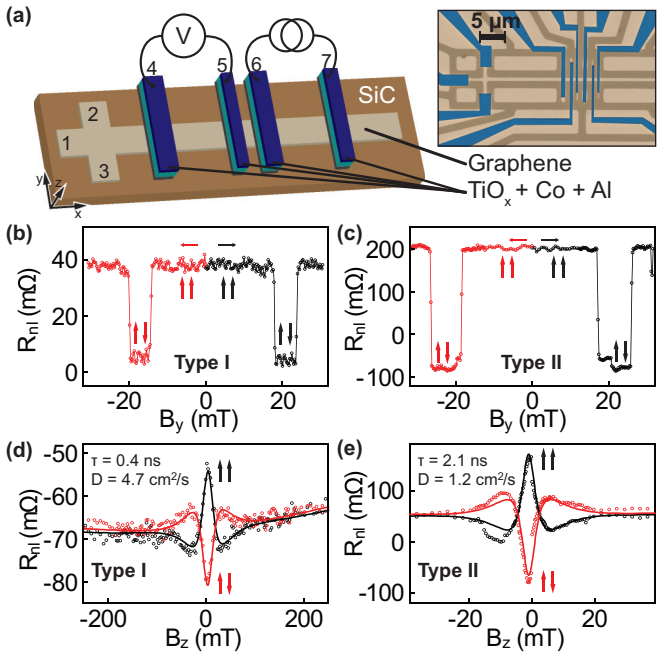

FIG. 2. (Color online) (a) Device schematics of an EG on SiC nonlocal spin valve with four spin contacts made of a TiO_2 tunnel barrier, Co, and an Al capping layer. The inset shows a colored microscopic image of the real device (type I) with a microscopic image of the etch lines (dark brown) superimposed. Additional lines were etched away in between the Co contacts to ensure there were no current paths outside the strip. (b), (c) RT spin valve measurements of EG by sublimation (type I) and CVD (type II). The distance L between the inner electrodes is 1 μm for both devices. The horizontal arrows represent the sweeping direction of the magnetic field. Vertical arrows show parallel or antiparallel orientation of the inner electrodes. The extra level in (c) is caused by the switching of one of the outer electrodes. The lines between measurement points are a guide to the eye. (d), (e) Hanle precession measurements at RT of type I and II in the parallel (black circles) and antiparallel (red circles) configuration. Note the large difference in the x-axis scales. The best fits are performed on a plot of $(R_{\mathrm{nl}}^{\uparrow\uparrow} - R_{\mathrm{nl}}^{\uparrow\downarrow})/2$ and inserted in this figure as black and red lines. Because of a small asymmetry in (e), the fit is performed only in the positive range of B_z. τ and D are obtained by fitting with the solution to Eq. (1) (see text).

in Figs. 2(d) and 2(e), we obtain a diffusion coefficient that clearly deviates from D_C. This modified value we denote as D^{mod}, giving 4.7 ± 0.4 and $1.2 \pm 0.1\ \mathrm{cm}^2\ \mathrm{s}^{-1}$ for type I and type II, respectively. The obtained relaxation time also seems to be modified, $\tau_{S1}^{\mathrm{mod}} = 400 \pm 30$ ps and $\tau_{S2}^{\mathrm{mod}} = 2.1 \pm 0.09$ ns, which is much higher than the typical $\tau_S = 200$ ps for exfoliated graphene.

The significant difference between D_C and D^{mod} is a clear indication that Eq. (1) does not hold, so we use the model from Ref. [6] for a more accurate explanation. This model assumes electronic states coupled to the channel that do not contribute to the charge transport. However, the states can contribute to the spin relaxation and precession. This happens when the coupling is strong enough and there are enough states contributing, a condition that can be described by the expression $\eta\Gamma \gg 1/\tau_S$. Here, Γ is the coupling rate between the channel and the localized states, $\eta = \nu_{\mathrm{ls}}/\nu_{\mathrm{graphene}}$ is the

ratio between density of states in the graphene and the density of localized states, and τ_S is the intrinsic spin relaxation time of the graphene, unaffected by the influence of the localized states.

The dynamics in the system are described by an effective Bloch equation [6],

$$\vec{0} = D\nabla^2\vec{\mu}_S - \frac{\vec{\mu}_s}{\tau_S^{\text{eff}}} + \vec{\omega}_L^{\text{eff}} \times \vec{\mu}_S. \tag{2}$$

Here, the effective relaxation time τ_S^{eff} and effective precession frequency ω_L^{eff} are given by

$$\frac{1}{\tau_S^{\text{eff}}} = \frac{1}{\tau_S} + \eta\Gamma\frac{1+\tau_S^*\Gamma+(\tau_S^*\omega_L^*)^2}{(1+\tau_S^*\Gamma)^2+(\tau_S^*\omega_L^*)^2} \tag{3}$$

and

$$\omega_L^{\text{eff}} = \omega_L + \eta\Gamma^2\frac{(\tau_S^*)^2\omega_L^*}{(1+\tau_S^*\Gamma)^2+(\tau_S^*\omega_L^*)^2}. \tag{4}$$

In the above expressions an asterisk $(*)$ is assigned to the corresponding properties of the localized states. Here, $\tau_S^{\text{eff}} = \tau_S^{\text{mod}}/\xi$ with $\xi \equiv D/D^{\text{mod}}$ [6]. Using $D = D_C$ we obtain $\xi_1 = 43$ and $\xi_2 = 143$.

The parameter space in this description includes seven quantities, D, τ_S, τ_S^*, g, g^*, Γ, and η, but we reduce that number by making some assumptions. First, we assume the properties of the graphene channel to be the same as the typical properties of exfoliated graphene with similar mobility: $D = 200\ \text{cm}^2\ \text{s}^{-1}$, $\tau_S = 150$ ps, and $g = 2$ [21]. We can make this assumption, because (1) we measured $D_C \approx D$ and (2) due to a weak spin-orbit interaction and the absence of electron-electron interaction we have no reason to expect a change in g. Then, assuming that (1) $g = g^* = 2$ and (2) the room temperature data are in the strong coupling limit, η is given by $\eta = \xi - 1 = D_C/D^{\text{mod}} - 1$ [6]. We can estimate τ_S^* under the same assumptions, and by using $1/\tau_S^{\text{eff}} = \xi/\tau_S^{\text{mod}} = 1/\tau_S + \eta/\tau_S^*$. The only unknown variable we are now left with is the coupling rate Γ.

An interesting question related to the nature of the coupling to the localized states is whether the process is mediated by temperature independent tunneling or hopping, which should be temperature dependent. Therefore, we cooled down the samples to liquid helium temperatures. We observed a distinct change in the line shape of the Hanle curve when cooling down. Figures 3(a) and 3(b) show the temperature dependence of the Hanle curve for both types. We plot here the spin signal $(R_{\text{nl}}^{\uparrow\uparrow} - R_{\text{nl}}^{\uparrow\downarrow})/2$ for each individual curve. At temperatures of 30 K and lower, the Hanle curve of type I in Fig. 3(a) evolves into a broader curve that does not cross zero and has an extra, narrow peak around zero field. This temperature dependence of the Hanle curve is surprising, as it was not seen before in EG by sublimation [1,3]. Type II in Fig. 3(b) behaves comparably, but also shows a decrease in amplitude at lower temperatures and the transition already takes place around 160 K. We were not able to accurately fit the anomalous Hanle data that arise at lower temperature. D takes on unrealistically high values due to the absence of a zero crossing and pronounced shoulders [17] and τ_S, typically associated with the width of the Hanle curve, becomes inaccurate, coming from the fact that the shape consists of a narrow peak on top of a broader curve.

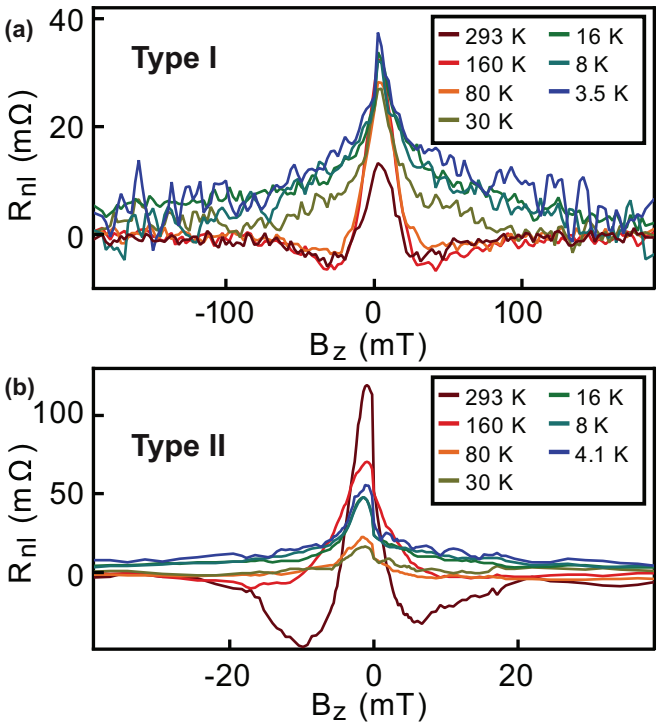

FIG. 3. (Color) Temperature dependent evolution of the Hanle curve. (a) EG by sublimation (type I). The typical RT Hanle line shape (dark red line) develops into a broader curve without zero crossings in R_{nl} and with a narrow peak around zero magnetic field at temperatures of 30 K and lower. (b) EG by CVD (type II). The Hanle line shapes change already at 160 K and also the amplitude decreases in the temperature range 293–30 K and increases again at 30–4.1 K.

Now we show in what regime of parameters these expressions can result in a Hanle curve with an anomalous shape. According to Ref. [6], τ_S^{eff} is approximately constant and ω_L^{eff} is linear with magnetic field in both the weak coupling regime $(\eta\Gamma \ll 1/\tau_S)$ and the strong coupling regime $(\eta\Gamma \gg 1/\tau_S)$. In both limits the Hanle curve has the same shape, but in the case of strong coupling the amplitude and peak width are reduced drastically. This explains the modified transport properties and the difference between D_C and D^{mod} that we typically see in EG at RT. Only in the transition regime $(\eta\Gamma \sim 1/\tau_S)$ does the full expression of Eqs. (3) and 4 come into play. A nontrivial line shape then arises from the fact that τ_S^{eff} becomes a function of ω_L and thus depends on B_z.

In Fig. 4 we model the development of the Hanle curve when entering the transition regime between strong and weak coupling. For these plots we use the solution to Eq. (2) and fill in Eqs. (3) and (4). We use the experimental results for D^{mod}, τ_S^{mod} [Figs. 2(d) and 2(e)], and $D = 200\ \text{cm}^2\ \text{s}^{-1}$ to estimate $\eta = 42\ (166)$ and $\tau_S^* = 0.42\ (2.3)$ ns for type I (II). In the weak coupling regime (blue curve) both Hanle curves follow the spin properties of the channel. In the model we assume these properties to be equal for both devices, so the blue curves in Figs. 4(a) and 4(b) are the same. In the intermediate regime, which is

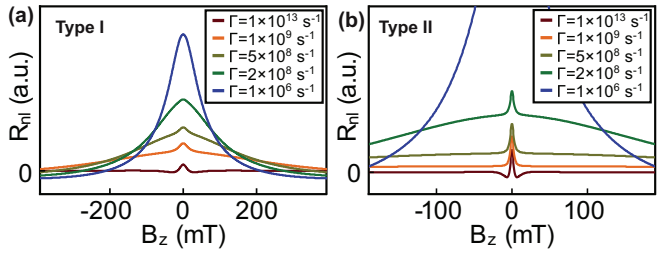

FIG. 4. (Color) Simulated curves for Hanle precession including the effect of localized states. The figures show the evolution of the Hanle line shape when changing the coupling rate Γ. For both plots we used $D = 200$ cm^2 s^{-1}, $\tau_S = 150$ ps, and $g = 2$. The blue curves show the weak coupling limit which is not influenced by the localized states and is therefore the same in both figures. (a) uses the estimated quantities τ_S^* and η of type I and (b) uses τ_S^* and η of type II.

around 20 ps $\leqslant 1/\eta\Gamma \leqslant$ 200 ps, the typical Hanle line shape changes into a superposition of a broad and a narrow peak. In the strong coupling regime (dark red lines) the shape is the same as a regular Hanle curve, but its amplitude and peak width both decrease drastically. In this regime the spin properties are dominated by the localized spin states, therefore $\tau_S^* \approx \tau_S^{\mathrm{mod}}$.

We now discuss how the simulated data from the localized states model relate to the experiment. When we compare Figs. 3 and 4 we see a similar double peak shape emerging when going from high to low temperature or from strong to weak coupling, respectively. The similarity of the two figures points to a coupling rate that is temperature dependent. This can be explained by two possible mechanisms: (1) The localized states are at the Fermi energy and the coupling is mediated by activated transport, where the thermal energy is used to overcome a tunnel barrier or (2) the localized states are distributed over a range of energies, depending on the available thermal energy. The strength of the effect is different for the two materials under investigation, EG by sublimation and EG by CVD. This can be explained by the structural difference of the buffer layer, resulting in a different density and/or energy distribution of the localized states.

When comparing the experiment and simulations we see a difference in ratio between the signal amplitude and curve width. This suggests more of the fitting parameters are temperature dependent, limiting the usefulness of Eq. (2) for fitting the experimental data. We also attempted to simulate the data using more free fit parameters. This, however, leads to a result with too many uncertainties of which the interpretation is unclear and an even higher value for η (see the Supplemental Material for the details of this analysis [14]). A possibility would be to incorporate a distribution of coupling rates similar to a so-called heavy tail distribution of trapping times that is seen in disordered semiconductors [22], which influences the Hanle shape even outside the intermediate coupling regime, according to Ref. [7]. Such an analysis might also shed more light on the high value we find for η, giving $\nu_{ls} = \eta\nu_{\mathrm{graphene}} \approx 2 \times 10^{13}\mathrm{eV}^{-1}\mathrm{cm}^{-2}$ or higher. This, however, is outside the scope of this Rapid Communication.

In short, we investigated a regime of intermediate coupling strength between diffusive and localized electron spins in EG on SiC and observed anomalous Hanle curves, giving insights in the effects that can play a role in widely used Hanle precession experiments. The interaction between the channel and localized states is complex, reflected in the number of variables in the model. Nonetheless, we found a qualitative agreement between the temperature dependence of the anomalous experimental Hanle curves and our model. We observed a significant difference in the density of localized states between the two material types, which is likely to be related to the structure of the buffer layer, the effect being stronger in EG by CVD. For both types, the analysis gives a high density of localized states in the buffer layer.

On the one hand, this work might provide answers for how to control transported spins by coupling them to their environment. On the other, it confirms the usefulness of spin transport to "read out" local spin properties.

We would like to acknowledge H. M. de Roosz, H. Adema, and J. G. Holstein for technical support and J. Fabian and P. J. Zomer for feedback on the manuscript. The research leading to these results has received funding from NanoNed, the Zernike Institute for Advanced Materials, and the European Union Seventh Framework Programmes under Grant Agreement "ConceptGraphene" (No. 257829) and "Graphene Flagship" (No. 604391).

[1] T. Maassen, J. J. van den Berg, N. IJbema, F. Fromm, T. Seyller, R. Yakimova, and B. J. van Wees, Long spin relaxation times in wafer scale epitaxial graphene on SiC(0001), Nano Lett. **12**, 1498 (2012).

[2] B. Dlubak, M.-B. Martin, C. Deranlot, B. Servet, S. Xavier, R. Mattana, M. Sprinkle, C. Berger, W. A. De Heer, F. Petroff, A. Anane, P. Seneor, and A. Fert, Highly efficient spin transport in epitaxial graphene on SiC, Nat. Phys. **8**, 557 (2012).

[3] B. Birkner, D. Pachniowski, A. Sandner, M. Ostler, T. Seyller, J. Fabian, M. Ciorga, D. Weiss, and J. Eroms, Annealing-induced magnetic moments detected by spin precession measurements in epitaxial graphene on SiC, Phys. Rev. B **87**, 081405 (2013).

[4] L. Xie, X. Wang, J. Lu, Z. Ni, Z. Luo, H. Mao, R. Wang, Y. Wang, H. Huang, D. Qi, R. Liu, T. Yu, Z. Shen, T. Wu, H. Peng, B. Özyilmaz, K. Loh, A. T. S. Wee, Ariando, and W. Chen, Room temperature ferromagnetism in partially hydrogenated epitaxial graphene, Appl. Phys. Lett. **98**, 193113 (2011).

[5] A. J. M. Giesbers, K. Uhlířová, M. Konečný, E. C. Peters, M. Burghard, J. Aarts, and C. F. J. Flipse, Interface-induced room-temperature ferromagnetism in hydrogenated epitaxial graphene, Phys. Rev. Lett. **111**, 166101 (2013).

[6] T. Maassen, J. J. van den Berg, E. H. Huisman, H. Dijkstra, F. Fromm, T. Seyller, and B. J. van Wees, Localized states influence spin transport in epitaxial graphene, Phys. Rev. Lett. **110**, 067209 (2013).

[7] R. C. Roundy and M. E. Raikh, Spin transport with dispersive traps: Narrowing of the Hanle curve, Phys. Rev. B **90**, 241202(R) (2014).

[8] C. Berger, Z. Song, T. Li, X. Li, A. Y. Ogbazghi, R. Feng, Z. Dai, A. N. Marchenkov, E. H. Conrad, P. N. First, and W. A. de Heer, Ultrathin epitaxial graphite: 2D electron gas properties and a route toward graphene-based nanoelectronics, J. Phys. Chem. B **108**, 19912 (2004).

[9] C. Virojanadara, M. Syvajarvi, R. Yakimova, L. I. Johansson, A. A. Zakharov, and T. Balasubramanian, Homogeneous large-area graphene layer growth on 6H-SiC(0001), Phys. Rev. B **78**, 245403 (2008).

[10] K. V. Emtsev, A. Bostwick, K. Horn, J. Jobst, G. L. Kellogg, L. Ley, J. L. McChesney, T. Ohta, S. A. Reshanov, J. Röhrl, E. Rotenberg, A. K. Schmid, D. Waldmann, H. B. Weber, and T. Seyller, Towards wafer-size graphene layers by atmospheric pressure graphitization of silicon carbide, Nat. Mater. **8**, 203 (2009).

[11] W. Strupinski, R. Bozek, J. Borysiuk, K. Kosciewicz, A. Wysmolek, R. Stepniewski, and J. M. Baranowski, Growth of graphene layers on silicon carbide, Mater. Sci. Forum **615–617**, 199 (2009).

[12] A. Al-Temimy, C. Riedl, and U. Starke, Low temperature growth of epitaxial graphene on SiC induced by carbon evaporation, Appl. Phys. Lett. **95**, 231907 (2009).

[13] W. Strupinski, K. Grodecki, A. Wysmolek, R. Stepniewski, T. Szkopek, P. E. Gaskell, A. Grueis, D. Haberer, R. Bozek, J. Krupka, and J. M. Baranowski, Graphene epitaxy by chemical vapor deposition on SiC, Nano Lett. **11**, 1786 (2011).

[14] See Supplemental Material at http://link.aps.org/supplemental/10.1103/PhysRevB.91.081403 for temperature dependent Hanle measurements on a second type II device. Also, additional simulations of the Hanle curves are presented, showing the effect of using more free parameters.

[15] We avoided the use of any negative tone resist because this can leave problematic resist residue after exposure, leading to high contact resistances and low polarization.

[16] G. Schmidt, D. Ferrand, L. W. Molenkamp, A. T. Filip, and B. J. van Wees, Fundamental obstacle for electrical spin injection from a ferromagnetic metal into a diffusive semiconductor, Phys. Rev. B **62**, R4790 (2000).

[17] T. Maassen, I. J. Vera-Marun, M. H. D. Guimarãs, and B. J. van Wees, Contact-induced spin relaxation in Hanle spin precession measurements, Phys. Rev. B **86**, 235408 (2012).

[18] We note that in our device geometry the Hall measurement probes a small EG region close to, but not exactly at, the spin channel.

[19] Epitaxial graphene on SiC is known to be heavily n doped. Hall characterization of the full 5×5 mm graphene sample yielded values of $2 - 6 \times 10^{12}$ cm^{-2} .

[20] We obtained the charge diffusion coefficient D_C using the Einstein relation $D_C = 1/[R_{\rm sq} e^2 \nu(E_F)] = \sqrt{\pi/(g_s g_v n)}\hbar v_F/(R_{\rm sq} e^2)$, where $R_{\rm sq}$ is the square resistance, e the electron charge, $\nu(E_F)$ the density of states at the Fermi level, the valley and spin degeneracy g_v and g_s are equal to 2, the Fermi velocity $v_F \approx 10^6$ m s^{-1}, and n the charge carrier density.

[21] N. Tombros, C. Jozsa, M. Popinciuc, H. T. Jonkman, and B. J. van Wees, Electronic spin transport and spin precession in single graphene layers at room temperature, Nature (London) **448**, 571 (2007).

[22] T. Tiedje and A. Rose, A physical interpretation of dispersive transport in disordered semiconductors, Solid State Commun. **37**, 49 (1981).